Continental Shelf Research 262 (2023) 105026

Contents lists available at ScienceDirect

Continental Shelf Research

journal homepage: www.elsevier.com/locate/csr

Dating recent tidal marsh sediments using windborne giant particles of green petcoke – An example from the southwest coast of Portugal

J. Moreno [a,*], E. Leorri [b], F. Fatela [a,c], M.C. Freitas [a,c], F. Moreno [d], J. Mirão [e], L. Dias [e], M. Leira [f], P. Masqué [g,h], A. Russo [a], A. Cunha [c], M. Inácio [c], W.H. Blake [i]

[a] Universidade de Lisboa, Faculdade de Ciências, Instituto Dom Luiz (IDL), 1749-016, Lisboa, Portugal
[b] Department of Geological Sciences, East Carolina University, Greenville, NC, 27858-4353, USA
[c] Departamento de Geologia, Faculdade de Ciências, Universidade de Lisboa, 1749-016, Lisboa, Portugal
[d] Independent Researcher, Caminho da Portela, n.° 97, 4940-061, Bico PCR, Portugal
[e] Laboratório HERCULES, IIFA, Universidade de Évora, Largo Marquês de Marialva, 8, 7000-809, Évora, Portugal
[f] Departamento de Bioloxía, Universidade da Coruña, Campus da Zapateira, 15071, A Coruña, Spain
[g] School of Science and Centre for Marine Ecosystems Research, Edith Cowan University, Joondalup, Western Australia, 6027, Australia
[h] International Atomic Energy Agency, 4a Quai Antoine 1er, 98000, Principality of Monaco, Monaco
[i] School of Geography, Earth and Environmental Sciences, Plymouth University, Plymouth, Devon, PL4 8AA, UK

ARTICLE INFO

Keywords:
Petroleum coke
Harbour (storage) facilities
Wind-induced fugitive dust emissions
Atmospheric transport
Salt marshes
Sediment cores
Anthropogenic time marker

ABSTRACT

Coastal systems are especially vulnerable to human activities resulting from a range of direct physical modifications of the ecosystems to the biological, chemical, and physical impacts of pollutants. For the most recent decades, these modifications can be accurately tracked by industrial development indicators, providing an exceptional record of historical changes. In return, when such changes are identified in the sedimentological record, they can serve as precise chronological markers. Here, we examined the potential of petcoke particles, a by-product of crude oil refining, as an emergent sediment dating tool. To this end, giant (63–~200 μm) black spheroidal petcoke particles – present in cores retrieved in the salt marshes of the Sado estuary (SW Portugal) – were used. These anthropogenic particles were counted and identified according to their morphology, structure, and chemical composition, using complementary micro-beam techniques: Scanning Electron Microscope and Energy Dispersive Spectroscopy, and Micro X-Ray Diffraction. The analyses revealed shot-type green petcoke particles containing a set of elements, which are well-known metallic/non-metallic impurities in petcoke. Based on the available historical data on petcoke imports in the port of Setúbal (Sado estuary) and Portugal, their first appearance in sediments can be dated to 1996 ± 2, with maxima in 2006 ± 4. Both the presence and the historical evolution of the use of petcoke in the region were recorded in all sediment cores, with higher particle density in locations aligned with the prevailing winds. The combination of petcoke and ^{137}Cs data provided accretion rates for the 1963–2006 period ranging from 0.1 to 0.3 cm yr^{-1} (average: 0.2 cm yr^{-1}), while these rates significantly increased from 2006 onwards (avg. rate: 1.1 cm yr^{-1}; range: 0.6–2.1 cm yr^{-1}). The widespread handling of petcoke worldwide leads us to suggest petcoke particles as a reliable chronological marker at local and regional scales, to be used in combination with other dating methods to build more exact sediment chronologies.

1. Introduction

A better understanding of historical environmental changes (natural and human-induced) is crucial to assess the status of the different ecosystems, forecasting responses to pressures from anthropogenic activities, and evaluating the efficiency of management actions. Coastal systems store large quantities of sediments that both accumulate pollutants and serve as archives of those environmental changes (e.g., Cearreta et al., 2000, 2002). In order to provide accurate chronologies for historical changes at high resolution, a combination of techniques and historical data from global, regional, and local sources is required. In fact, the pollutants recorded in the sediments can be used as

* Corresponding author.
E-mail address: jcmoreno@fc.ul.pt (J. Moreno).

https://doi.org/10.1016/j.csr.2023.105026
Received 30 December 2022; Received in revised form 6 May 2023; Accepted 12 May 2023
Available online 21 May 2023

chronological markers that allow precise temporal reconstructions otherwise not always feasible. One such marker is Cesium-137 (^{137}Cs). This anthropogenically introduced radioisotope (half-life: 30.05 ± 0.08 years) serves as a global marker in response to nuclear testing with a distinct maximum peak in 1963 (see, for instance, Appleby, 2008 and regional examples from coastal marshes, such as García-Artola et al., 2016; Moreno et al., 2017). In some instances, the use of Cesium-137 is controversial due to its potential vertical mobility, sediment mixing, or transport/erosion (Milan et al., 1995), but despite these limitations, it has been widely used to support ^{210}Pb chronologies (e.g., Lu and Matsumoto, 2005; Appleby, 2008; Leorri et al., 2014a; Kemp et al., 2017; Olszewski et al., 2018; Buffoni et al., 2020). Other chronological markers derived from anthropogenic activities of regional or global relevance have been incorporated into the age-depth models to constrain the environmental histories recorded in sediments of aquatic systems. Lead (Pb) concentrations depart from sediment background values in response to industrial activities, e.g., in the north of the Iberian Peninsula at AD 1900 (e.g., García-Artola et al., 2015; Irabien et al., 2015) and peak in the same region in 1975 (Leorri et al., 2014a; García-Artola et al., 2015). Polycyclic aromatic hydrocarbons (PAHs), together with Pb stable isotopes, also provide reliable alternative chronologies of past events that can be used in the sediment to comprehend environmental changes (e.g., Leorri et al., 2014b). These signals in the sedimentological record sometimes seem to be coeval globally, although local and regional emissions provide geographically limited but stronger signals (Leorri et al., 2014b), with small but clear chronological differences. In addition to the atmospheric transport of pollutants, sediments also record local discharges resulting from intense industrial activity (e.g., Cearreta et al., 2000, 2002; Irabien et al., 2015) or reflect agricultural land uses (e.g., García-Artola et al., 2016) that can support the development of an accurate chronology. Within this context, the knowledge of the local contamination history and the preservation potential of salt marsh sediments can provide adequate tools to improve our understanding of sedimentological processes and contribute to interdisciplinary research aimed at increasing the available set of sediment dating methods. Such research needs to ensure the most suitable tracers and a possible candidate is petroleum coke (petcoke).

Petcoke is a by-product of the coking processes used in petroleum refineries during crude oil refining. Coking initially converts petroleum residuum into lighter-range hydrocarbons, low-Btu gas, and coke (Mancuso and Arienti, 2017). This raw coke (green coke) can be used either directly as a fuel or undergo further thermal processing (calcination) to remove any residual (heavy) hydrocarbon (also termed volatile matter) and increase the percentage of elemental carbon (C). In the calcining process, green coke is heated to temperatures greater than 1200 °C, producing calcined petcoke (e.g., Caruso et al., 2015; Edwards, 2015). Petcoke (both green and calcined) is a carbonaceous hydrophobic grey to black-coloured solid. The majority is a hard glassy substance that resembles coal, although a small fraction is made up of carbonaceous fibres (Maxim et al., 2006). Concerning physical properties, it may be classified as shot coke, needle coke, and sponge coke, these various forms with different (complex) microstructures (API, 2008; Edwards, 2015). Green petcoke has a variable chemical composition, depending on the original crude oil, feedstocks for the thermal decomposition process, and coking operation conditions (McKee et al., 2014). Typically, almost 90% (by mass) of raw/green coke is composed of C (80–95%), while hydrogen (3.0–4.5%), nitrogen (0.1–0.5%), oxygen (1.3–2.1%), and sulfur (0.2–6.0%) represent most of the rest (Mancuso and Arienti, 2017). Petcoke also contains other elements (i.e., impurities/contaminants) that can occur within wide ranges, such as iron (50–2000 ppm), vanadium (5–5000 ppm), and nickel (10–3000 ppm) (CONCAWE, 1993), these two – V and Ni – used to classify the source of oil (Barwise, 1990; López and Lo Mónaco, 2017). Calcined coke (which is 98.0–99.5 wt% C) has physicochemical properties and chemical composition analogous to green coke, the main difference between the two is the content of residual hydrocarbons, normally 0.2–0.8% vs. 5–15% (Mancuso and Arienti, 2017). The bulk densities for green coke and calcined coke are 0.80–1.40 g cm^{-3} and 0.80–0.88 g cm^{-3}, respectively (Lee et al., 1997), while their respective real densities are 1.35–1.45 g cm^{-3} and 2.06–2.16 g cm^{-3} (CONCAWE, 1993).

Due to its relatively low cost compared to coal, there has been an increasing global demand for petcoke supply in a wide range of industries (Stockman, 2013). Petcoke is used primarily as a fuel source and to provide energy for industrial combustion processes, such as cement manufacturing (Andrews and Lattanzio, 2013). Higher grades of calcined coke have non-energy applications, namely in the production of electrodes, particularly required in the aluminium, steel, and titanium smelting industries (e.g., Caruso et al., 2015; Kameshkov et al., 2021). The usage of petcoke as a valued international commodity for decades led to its outdoor storage in port terminals around the world, where it was kept until transferred to (end) users. For this reason, the presence of huge amounts of petcoke in uncovered piles at dry bulk cargo terminals has become pervasive, with atmospheric emissions potentially resulting in residential exposure through inhalation of fugitive petcoke dust and dermal exposure (Caruso et al., 2015; Dourson et al., 2016). Once in the aquatic milieu, petcoke settles through the water column, being incorporated into the sediments, where it can persist because chemically (and physically) petcoke is considered essentially inert (e.g., Andrews and Lattanzio, 2013). Therefore, the presence of airborne anthropogenic petcoke in sedimentary records of surface aquatic systems has the potential, in theory, to be an appropriate local or regional geochemical/chronological indicator and a proxy for sedimentological processes.

It is important to mention that spheroidal carbonaceous particles (SCPs) are morphologically and chemically analogous to petcoke and both can be mistakenly identified with each other. Spheroidal carbonaceous particles are a fly ash product of industrial combustion of fossil fuel (coal-series; fuel-oil) at elevated temperatures (T > 1000 °C) and are emitted to the atmosphere along with flue gases (e.g., McCrone and Delly, 1973; Bacci et al., 1983; Rose et al., 1999, 2003; Rose, 2015). The high temperatures (1650 °C) reached during the combustion of heavy fuel oil are associated with high-temperature minerals formation (e.g., Shawabkeh et al., 2011; Al-Degs et al., 2014; Basha et al., 2020), present in fly ash particles. On the other hand, green petcoke is produced in petroleum refining operations at lower temperatures (415 °C–505 °C, at high pressures of 90 psi; Petroleum Coke Group, 2020). Through the presence of high-temperature minerals (e.g., Mullite, $Mg_3V_2O_8$, $PbSO_4$), petcoke and SCPs can be differentiated. Moreover, while petcoke (in this study) is limited to particles >63 μm, the usual size range of SCPs in the environment is 2–20 μm (diameter), although the largest particles can reach >50 μm. It is especially relevant to identify these differences, considering that SCPs have also been used as chronological markers (e.g., Rose and Appleby, 2005). Specifically, SCPs are anthropogenic by-products (e.g., Ruppel et al., 2013), resulting in an unambiguous marker of anthropogenic fossil fuel combustion and a record of the unprecedented impact of human activity on the environment (e.g., Swindles et al., 2015). The rapid increase of the global SCP, signalling the mid-20th century in lacustrine and marine sediments, peats, and ice cores, has been proposed as a marker for the onset of the Anthropocene (Rose, 2015). But the SCP concentration peak (similarly to petcoke) can vary spatially, reflecting proximity to pollution sources (Swindles et al., 2015), the introduction of particle arrestor technology to combustion sources, changes to alternative fuel types (e.g., from coal to natural gas), regional changes of heavy industry (Rose, 2015), or temporally, exhibiting delays in the acceleration of industrialization (Inoue et al., 2022).

The Sado estuary (SW Portugal) is considered as moderately contaminated, being impacted by various anthropogenic activities, from shipping, industry, urban development, agriculture, and mariculture (Pereira et al., 2014). Even though some research has been carried out in this estuary to assess metal contamination, as a local fingerprint of anthropogenic activities (e.g., Caeiro et al., 2005; Freitas et al., 2008; Moreira et al., 2009; Serafim et al., 2013), most of the studies focused on

Fig. 1. Study site location within the Sado estuary (SW Portugal) (A), showing the surrounding solid bulk terminals (Sapec and Eurominas/Termitrena), the cement factory (Secil), and the locations of the seven cores: FAR4A and FARW1.6 (northern margin), CARW1.5 (southern margin), and CTAS9, MCN5A, MCS4B, and TCN3A (Tróia back spit) and the modeled yearly wind frequency directions (https://globalwindatlas.info) (B). On the right (C), at the top, is a perspective of the Eurominas/Termitrena terminal (https://www.portodesetubal.pt/terminais_portuarios.htm); below, is a Google Earth image from the uncovered stockpiled petcoke at this terminal (21/01/2020).

the impact of pollutants in sediments on the biological ecosystems or human health (e.g., Costa et al., 2011; Lillebø et al., 2011). To the best of our knowledge, no work has been carried out to date on the recognition of the atmospheric dispersion of pollutants in the sediments of the Sado estuary with a focus on its use as a chronological marker, nor on the reconstruction of the chronology of pollution in this coastal environment, namely, that related to fossil fuels. In this direction, the aim of the current work was to investigate the usefulness of petcoke as a dating tool for recent sediments in the Sado estuary and to assess the preservation potential of high marsh sediments in the region. For that, we considered the historical concentrations of petcoke in seven high marsh sediment cores recovered in the estuary and compared them with both the available information on the industrial use of petcoke in the surrounding area and the sedimentary records of ^{210}Pb and ^{137}Cs. The objective was twofold: (i) to provide an accurate chronological marker that would support other techniques (e.g., ^{210}Pb, ^{137}Cs) for dating century-old sediments, which could be successfully applied in estuaries that have been repositories of this material; and (ii) to obtain short-term (defined here as less than 10–15 years) sedimentation rates.

2. Study area

The Sado estuary, on the southwest coast of Portugal (Fig. 1A), is the second-largest Portuguese estuary, with an area of approximately 24,000 ha. Located in the Mediterranean biogeographic region, most of the estuary is classified as a Nature Reserve. Regardless of this classification, it is home to many important industries, particularly on the northern margin (Fig. 1B). Furthermore, the estuary has received discharges of urban wastewater from the city of Setúbal (115,126 residents; INE, Instituto Nacional de Estatística, 2019), the port of Setúbal and associated activities, including fugitive emissions of dusty materials (Almeida et al., 2012), and effluents from the industrial settlements in the Sado River basin. In other areas around the estuary, intensive agriculture (mainly rice and tomatoes) is the main land use, along with traditional salt pans and an increasing number of fish farms (e.g., Caeiro et al., 2009; Gonçalves et al., 2015; Cabrita et al., 2020).

The estuary is a shallow basin (an average depth of 8 m) enclosed by a sand spit, with a maximum depth of 50 m in the inlet channel (Freitas et al., 2008). The flooded area at high water is about 150 km^2 and extends NW-SE upstream for 37.5 km to Alcácer do Sal, and in the NNE-SSW direction for 25 km to Águas de Moura and Comporta (Fig. 1B). The tidal inlet, ~2 km wide, is limited by the northern end of the Tróia sand spit and the Arrábida mountain, and its narrow entrance prevents the propagation of ocean waves into the inner estuary. The inlet channel bifurcates upstream into two – the North channel (flood-dominated) and the South channel (ebb-dominated), which are separated by several aligned sandbars. The Sado estuary is high-mesotidal near the mouth, with a tidal range of ~1.3 m (neap tides) and 3.5 m (at spring water); this range increases upstream, reaching a maximum of 4.1 m at mean high spring tide (MHWS) ~26 km inland (Montalvo). The spring tidal prism is 3.8 × 10^6 m^3 and the tidal currents dominate the estuarine dynamics, a consequence of both the limited inflow of freshwater from the Sado River and the negligible flow of the Marateca and Comporta streams, also discharging to the estuary (Águas de Moura and Comporta channels, respectively). Thus, the salinity remains close to that of typical seawater (slightly above 30‰), with a considerable part of the estuarine bottom covered by sandy sediments of marine origin. The upper reaches are fringed by intertidal mudflat and marsh habitats, occupying about a third of the estuary and reflecting low energy conditions in sheltered areas (Freitas et al., 2008).

The port of Setúbal infrastructure is concentrated on the northern margin of the estuary (Fig. 1B). It comprises specialized (public and private) terminals, such as those of several industrial facilities (see Fig. 1B and C). Among them, five are assigned to solid bulk cargo (e.g., Eurominas; Fig. 1C). Since the mid-1990s (APSS, SA – Administration of Ports of Setúbal and Sesimbra; unpublished data), the port has received coke from ships, which is unloaded, stored outdoors in large open-air stockpiles, and then delivered by heavy trucks to various industrial facilities located in the vicinity of Setúbal (e.g., cement plants, pulp mill and paper mills, ship repair, minerals, metal processing, production of fertilizers, chemical products). The black stockpiles of petcoke (8–10 m high; Fig. 1C), left uncovered in part due to the need for frequent material transfer, are prone to different wind erosion mechanisms, causing material loss from piles and dispersal and resuspension of dust in the ambient air. This leads to increased atmospheric particulate matter (PM) concentrations, with considerable health hazards when particles are transported to urban areas (e.g., Novak et al., 2015). Moreover, it has been demonstrated that, like the surfaces of stockpiles, the ground areas around piles can be (secondary) sources of settled dust, contributing appreciably to the total emission of dust particles from external storage areas (Furieri et al., 2014).

According to data from the local meteorological station (170 –

Table 1
Sediment core data from this study (location, collection year, corer type, the core length, and elevation in relation to mean sea level – m.s.l.).

Core	Location	Collection year	Corer	Length (m)	Elevation (m)
FAR4A	38°31′05.34″N; 8°47′03.62″W	2005	van der Horst	0.76	1.53
CARW1.5	38°24′41.43″N; 8°45′32.10″W	2010	Auger	1.00	2.18
FARW1.6	38°31′05.37″N; 8°47′02.97″W	2010	Auger	1.00	1.73
CTAS9	38°29′24.18″N; 8°53′46.24″W	2016	van der Horst	1.39	1.38
MCN5A	38°26′41.80″N; 8°49′55.07″W	2018	van der Horst	1.87	1.54
MCS4B	38°25′13.83″N; 8°49′05.01″W	2018	van der Horst	1.50	1.54
TCN3A	38°23′54.04″N; 8°48′12.82″W	2020	van der Horst	2.04	1.58

Setúbal: Lat.: 38° 32′ N; Lon.: 08° 53’ W; Alt.: 35 m m.s.l.), the most common wind directions were blowing from the NW and during the winter between the N and W quadrants (1961–1990 period; PROMAN, 2016). The mean annual wind speed was 6.9 km h^{-1}, with the highest monthly average speed – 8.4 km h^{-1} in August – coming from NW. With a frequency of 39.4%, the NW trend was the dominant wind direction, followed by northerly winds (16.5%). The average annual characteristics of the wind regime were generally maintained throughout the year, with small differences registered only during the winter period – regarding the frequency distribution – and during the summer period – in the amplitude of wind speeds (PROMAN, 2016).

3. Materials and methods

3.1. Sampling and analytical techniques

3.1.1. Sediment coring

Seven sediment cores were retrieved between 2005 and 2020 from the fringing salt marshes of the Sado estuary (Fig. 1B; Table 1), using either a van der Horst or an Auger sampler. At each sampling site, several (2–5) replicate cores were collected. The sampling sites are in the vegetated high marsh zone of both margins: Tróia spit (southern margin) – CTAS9, MCS4B, MCN5A, and TCN3A; Mitrena (northern margin) – FAR4A (Freitas et al., 2008), FARW1.6; and Carrasqueira (southern margin): CARW1.5. All sampling sites are within a 10 km radius of the open coke stockpile storage facilities at the port of Setúbal (Eurominas/Termitrena terminal; Fig. 1B and C). Here we focus on the signature of anthropogenic activity (illustrated by the presence of petcoke particles) in recent intertidal sediments. The core-top sediments were sampled every 1 cm (except FAR4A, sampled at 2 cm resolution) to obtain a high resolution of the sedimentary record. The aliquots of bulk sediment (1 cm thick slices; n = 160) were weighed before and after oven dried at 50 °C. For petcoke analysis, samples were wet sieved to remove clays and silt and retain the fraction >63 μm. Next, petcoke particles (>63 to ca. 200 μm) were counted, using a sorting tray with a gridded insert under a binocular microscope Olympus SZX12 (magnifications from 10x to 135x). When fragments were present only those greater than one-half of a spheroidal petcoke particle were counted. Selected petcoke particles were wet-picked, with a micropipette, from each sample for imaging, chemical, and mineralogical analysis. Next, the sediment was dried and weighed. The concentration of petcoke particles >63 μm was calculated as the number of particles >63 μm per gram of total dry sediment (g^{-1} dry wt.).

The organic matter content was estimated from Loss-on-Ignition (LOI; Table S1), with an aliquot of bulk sediment sample (2.0 g) dried and oven-heated at a temperature of 500 °C ± 50 °C for about 2 h (Moreira et al., 2009). Quality control was performed through replicates (n = 2) on 40% of the samples.

3.1.2. Radiometric analyses

^{210}Pb and ^{137}Cs activities were determined for six high marsh cores to assess the sedimentological processes (e.g., sediment mixing, sedimentation rates, preservation potential). Cores MCN5A, TCN3A, and CARW1.5 were analysed at 1 cm resolution, while cores CTAS9 and FAR4A were analysed at 2 cm intervals, and core MCS4B was based on low-resolution sampling at 4 cm intervals. Core FARW1.6 was not analysed for radionuclides, but sedimentation rates were assumed to be equivalent to that obtained from nearby core FAR4A. ^{210}Pb profiles and the ^{137}Cs 1963-maximum peak were used to inform the preservation potential, sediment mixing, sedimentation rates, and mass accumulation rates (when possible) of each sediment core. Cores CTAS9 and MCS4B (analysed at the Department F.-A. Forel of the University of Geneva, Switzerland), and FAR4A (analysed at the Environmental Sciences Department, Bordeaux University, France), were analysed by gamma spectrometry, as described in Freitas et al. (2008) and Inácio et al. (2022). Core CARW1.5 was also analysed by gamma spectrometry at the Earth and Environmental Sciences Department, Plymouth University, UK (see Leorri et al., 2010, 2013, for the description of the methods). Cores TCN3 and MCN5A were analysed by gamma spectrometry for ^{137}Cs, while ^{210}Pb was determined through the analysis of ^{210}Po by alpha spectrometry (Sanchez-Cabeza et al., 1998) at the School of Science of Edith Cowan University, Australia. In all cases, ^{137}Cs was determined by its gamma emissions at 662 keV. The concentrations of excess ^{210}Pb for each core were determined as the difference between total ^{210}Pb (from either gamma or alpha spectrometry) and ^{226}Ra (equivalent to supported ^{210}Pb), determined by gamma spectrometry via its decay products in equilibrium at the time of counting, ^{214}Pb, and ^{214}Bi. The results of ^{137}Cs and ^{210}Pb (Bq/kg) are presented in Table S2.

3.1.3. Imaging and geochemical analyses

3.1.3.1. Coke morphology and elemental analysis. The direct observation of the individual petcoke particles was conducted in 160 samples, with a binocular microscope Olympus SZX12 (magnifications from 10x to 135x), and at high magnification, using a variable-pressure scanning electron microscope (VP-SEM). Scanning electron microscopy (SEM) coupled to an energy-dispersive X-ray spectroscopy (EDS) system was used to image and characterize the particles in a subset of 36 samples, providing a semi-quantitative chemical elemental composition. The SEM-EDS analyses were performed at HERCULES Laboratory, University of Évora, taking a total of 129 measurements on very small areas of multiple discrete particles, using a Hitachi S3700N equipped with an X-ray spectrometer Bruker XFlash® 5010 SDD EDS Detector, with 129 eV spectral resolution at the FWHM/Mn Kα. The samples were analysed at a 40 Pa chamber atmosphere, 20 kV accelerating voltage, and a working distance of 6–11 mm, using the backscattered electron (BSE) detector. This analytical setup allowed the identification of particles with different compositions, by combining BSE imaging with EDS analysis. It also provided good-quality X-ray compositional maps. A secondary electron detector was applied to assess more detailed information on the surface of the particles. The errors of the analyses are at the 1 sigma level (±1σ [wt%]).

3.1.3.2. Micro X-ray diffraction (μXRD). Micro X-ray diffraction experiments were carried out directly on the petcoke particles picked up in the cored sediments, confirming their identity (or not) as petcoke. The μXRD is an invaluable technique usually used to examine either small or inhomogeneous samples, with strong composition gradients, providing direct information on the presence of phases, their crystallinity, and potential impurities in structures (Costa et al., 2019). Measurements were done with a commercial Brüker AXS D8 Discover diffractometer (DAVINCI design), using a Cu Kα radiation source, a 1 mm collimator, a

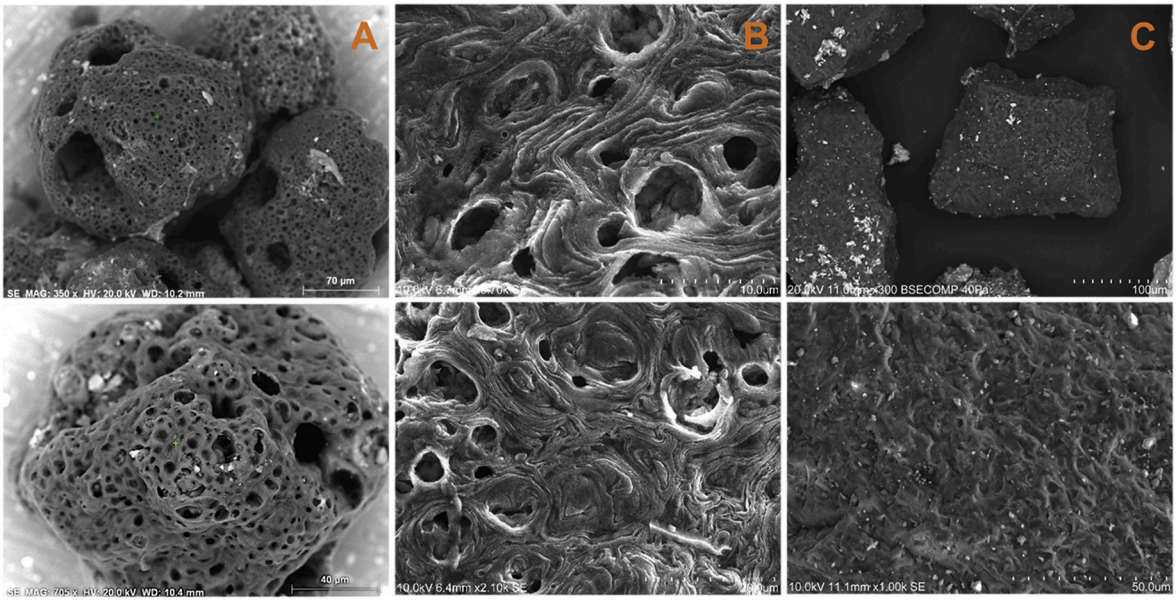

Fig. 2. SEM micrographs of representative samples. A) MCS4B_11–12 cm core sample; B) MCS4B_8–9 cm core sample (top) and FARW1.6_7–8 cm core sample (bottom); C) Eurominas stockpile sample.

LynxEye 1D detector, a Goebel mirror, a motorized XYZ stage, and operating with DIFFRAC.SUITE software package. Diffraction patterns were collected from 3 to 75° 2θ with a step of 0.05° and 2 s by step. The identification of the peaks was done using the Bruker EVA software with the International Centre for Diffraction Data Powder Diffraction Files (ICDD PDF) database.

4. Results and discussion

4.1. Characterization of the petcoke particles

Morphologically, the petcoke particles, exhibiting glassy granular spheroid shapes (e.g., sample MCS4B_11–12 cm; Fig. 2A), can be regarded as shot-associated type coke (e.g., Picón-Hernández et al., 2008). Such spheroidal morphologies are highly porous (large holes and pores) and dominated by a textured surface with etched, convoluted, layered structures (Fig. 2B). The macroporosity of these particles is much higher than that of petcoke currently stored at the Eurominas solid bulk terminal (Fig. 2C), which may have meaningful implications in terms of chemical composition and transport.

The μXRD results showed that the particles (shots and compacts) have a non-crystalline structure (see Fig. 3A), and this, combined with the EDS measurements obtained via SEM, confirmed a fully amorphous C-rich material, consistent with petcoke. Likewise, the relative abundance S > Si (excluding C) allows petcoke particles to be distinguished from other particles (e.g., ore) present in environmental samples (Zhang et al., 2016; Jariyasopit et al., 2018), a point also corroborated by the EDS results. Moreover, the absence of high-temperature minerals (μXRD analysis), such as Mullite ($3Al_2O_3{\cdot}2SiO_2$), magnesium orthovanadate ($Mg_3V_2O_8$), Anglesite ($PbSO_4$), associated with elevated temperature burnt fuel oil processes (e.g., Shawabkeh et al., 2011; Al-Degs et al., 2014; Basha et al., 2020), as previously stated, enabled us to differentiate our material (green coke) from SCPs. Fig. 3B shows, as an example, a standard EDS X-ray analysis for the petcoke particles found in the Sado sediments (core: MCS4B; Fig. 3B, top) and the stockpiled petcoke (Eurominas; Fig. 3B, bottom), and in which, besides the very prominent C peak, Al, Si, S, K, V, Fe, Cu, and Ca can be recognized. Additional chemical elements were identified in other Sado petcoke particles, namely Mg, Cl, Ti, P, Zn, Ni, Mn, Br, and Na (the concentrations for the analysed particles are given in supplementary material; Table S3). They are all known (micro)constituents of petcoke, corresponding to impurities/contaminants that are transferred during the processing of crude oil to the products obtained from petroleum (e.g., Tillman et al., 2012; Edwards, 2015; Kiciński and Dyjak, 2020). Two light rare earths – cerium and neodymium – were identified in white surface deposits, often coating single petcoke particles stored at the Eurominas terminal (Fig. 2C, the top SEM image; results not shown). In general, the C values were relatively high, ranging from 62.1 to 94.5 wt% (mean value: 80.8 wt%). Even so, in a few analyses (n = 16), the EDS technique provided at least one result below the cutoff of 80 wt% C (Table S3). A plausible explanation is that the microporosity and vesicular texture of the shots may have acted in such particles as a sediment trap, which was mirrored by higher Al and Cl (Table S3), together with a lower C wt%. Overall, the chemical signature of the petcoke particles observed in the Sado high marsh sediments is the following: high content of Al (avg. 10.5 wt%; min.–max. 0.10–19.2 wt%), S (4.7 wt%; 1.0–8.9 wt%), and V (0.28 wt%; 0.12–0.53 wt%). It is noteworthy that no Ni was identified (limit of detection, LOD: 0.2–0.3%) in most analyses (n = 127; 98.4%), even in the particles sampled at the Eurominas terminal (n = 6). Although Ni is a characteristic impurity in petcoke, there are large differences between previously published values (of three orders of magnitude, as mentioned earlier), with variability primarily related to the crude oil or feedstock composition (e.g., Lewan, 1984; CONCAWE, 1993; Tillman et al., 2012; McKee et al., 2014; López and Lo Mónaco, 2017; Petroleum Coke Group, 2020). Consequently, the analytical sensitivity of the method (high LOD) would not allow the detection of a substantial range of Ni levels in petcoke.

4.2. Petcoke incorporation in the sediments and implications as chronological markers

4.2.1. Regional historical use of petcoke, chronology, local sources, and potential pathways for transport

The Sado estuary has a long history of industrialization that began at the end of the 19th century, related to the cement and fertilizers industries (e.g., Quintas, 2011). Since the 1970s, the industrial activity in the estuarine area has increased significantly and the port of Setúbal has expanded as part of its development (e.g., Dias and Alves, 2010; Quintas, 2011). The industries with the greatest environmental impact have been those involving pulp and paper, chemicals, pesticides, fertilizers, yeast,

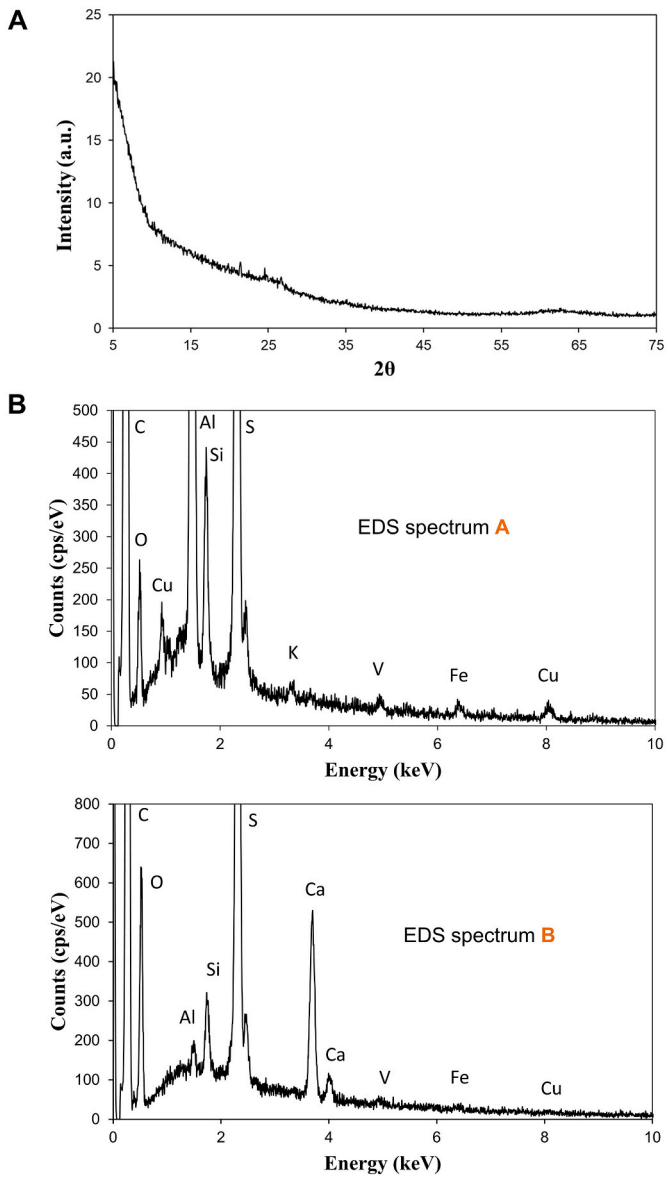

Fig. 3. A) Micro X-ray diffractogram (FAR4A_3–4 cm core sample); B) EDS spectra, obtained from the SEM-EDS analysis: Spectrum A – MCS4B_11–12 cm core sample; Spectrum B – Eurominas stockpile sample.

food, shipyards, mining-related industries, and port-related activities (e.g., Caeiro et al., 2005), all major consumers of fossil fuels, viz., coal and coke. The high sulfur content (average: 4.7 wt%) found in the petcoke present in the Sado high marsh sediments strongly suggests that it is green coke for co-combustion (fuel) purposes (e.g., Santos et al., 2015).

The data on coal and coke unloaded at the port of Setúbal from the Administration of Ports of Setúbal and Sesimbra (APSS, SA) and Portuguese imports of petcoke (data from the United Nations; http://data.un.org) are presented in Fig. 4. The two historical datasets are directly correlated: linear r (Pearson) = 0.82 and Spearman's r = 0.87 ($p < 0.05$). They evidence an important increase (of ~1.9 times in the port of Setúbal; and of ~3 times in Portugal) in the late-1990s (1997/98) compared to the early 1990s, with higher imports during the 2000s (peaks: 2004/05; 2008–2010) and a clear reduction (of ~1.4 times) at the end of this decade, followed (2011 onwards) by statistically significant decreasing trends (in both port of Setúbal and national imports; Mann-Kendall test; $p < 0.05$). Most of the cement industry was fueled by coal combustion in the early 1990s, undergoing a transition between 1998 and 2005, with the replacement of coal by petcoke, subsequently

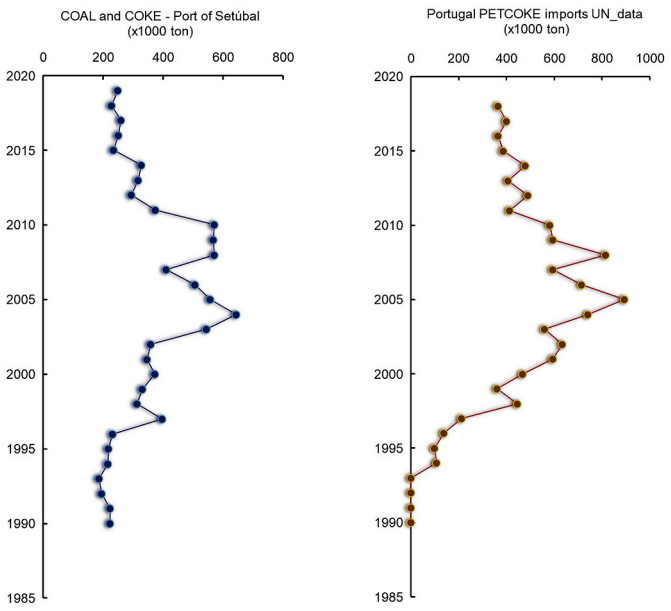

Fig. 4. Data on imports of coal and petcoke. Left: historical trends of coal and coke unloaded at the Port of Setúbal (source: APSS, SA – Administração dos Portos de Setúbal e Sesimbra); Right: Portuguese petcoke imports (data from the United Nations; http://data.un.org/Data.aspx?d=EDATA&f=cmID%3APK, accessed in 22/10/2020).

increasing the share of natural gas consumption, which by 2020 accounted for 50% of the energy consumed, with coke representing around 30% (Pereira et al., 2020). Factors, such as effectiveness in implementing environmental regulations, energy conversion from cement plants, and the 2008 global financial crisis (e.g., Lin et al., 2013) contributed to the decline in petcoke imports.

The amount of dust emission (natural and human-derived) is affected by a wide array of factors among them meteorological conditions (e.g., wind direction and speed; precipitation), material characteristics (e.g., PM size distribution), control measures in place (e.g., windscreens, stabilizers, dust suppression), or the mechanical disturbance to which the material is exposed (e.g., EPA, 1978; Mueller et al., 2015; MOECC, 2017; Sorte et al., 2018). Once the dust is emitted, it will move away from the source again influenced by a variety of parameters, namely wind, precipitation occurrence, and dilution processes. Wind can carry airborne contaminants for thousands of kilometers to remote locations around the globe (Kuo, 2018). Among those contaminants, there is a myriad of carbonaceous particles, such as the SCPs – a clearly identifiable component of black carbon (e.g., Ruppel et al., 2013) – which have been recorded in lacustrine and marine sediments, ice cores, and surface snow samples far from industrialized regions (e.g., Doubleday et al., 1995; Rose et al., 1999, 2012; Bindler et al., 2001; Hicks and Isaksson, 2006; Martins et al., 2010; Barst et al., 2017). Coarse modes (PM over 10 μm diameter) have been reported to predominate in the dry deposition flux of atmospheric particles, particularly in zones close to emission sources, possibly being transported only on a regional scale (e.g., Jaenicke, 1980; Holsen and Noll, 1992). In addition, giant particles (63–~200 μm), such as those studied here, are expected to originate only from a local source (short-range transport), with the largest (≥100 μm) usually considered "saltators", and unlikely to be lifted above a few centimeters from the ground surface (Rosenberg et al., 2014). However, the presence of giant airborne particles has been observed in long-range transport over the Atlantic Ocean at 2400 km and 3500 km from the West African coast (e.g., Van der Does et al., 2018). Thus, it is expected that the giant petcoke particles deposited in the high marsh zone of the Sado salt marshes and preserved in the sediment cores (Fig. 4) come from sources on a local to regional scale (<100 km). Given this, the most

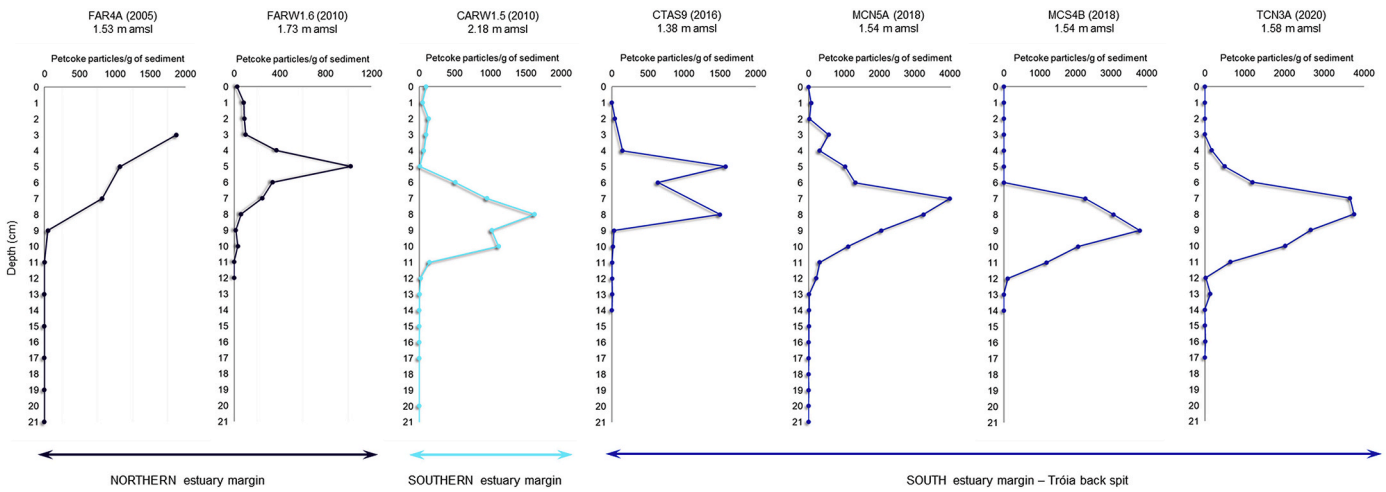

Fig. 5. Giant spheroidal petcoke particles (63–~200 μm) per gram of dry sediment in seven cores collected from 2005 to 2020 in the Sado estuary.

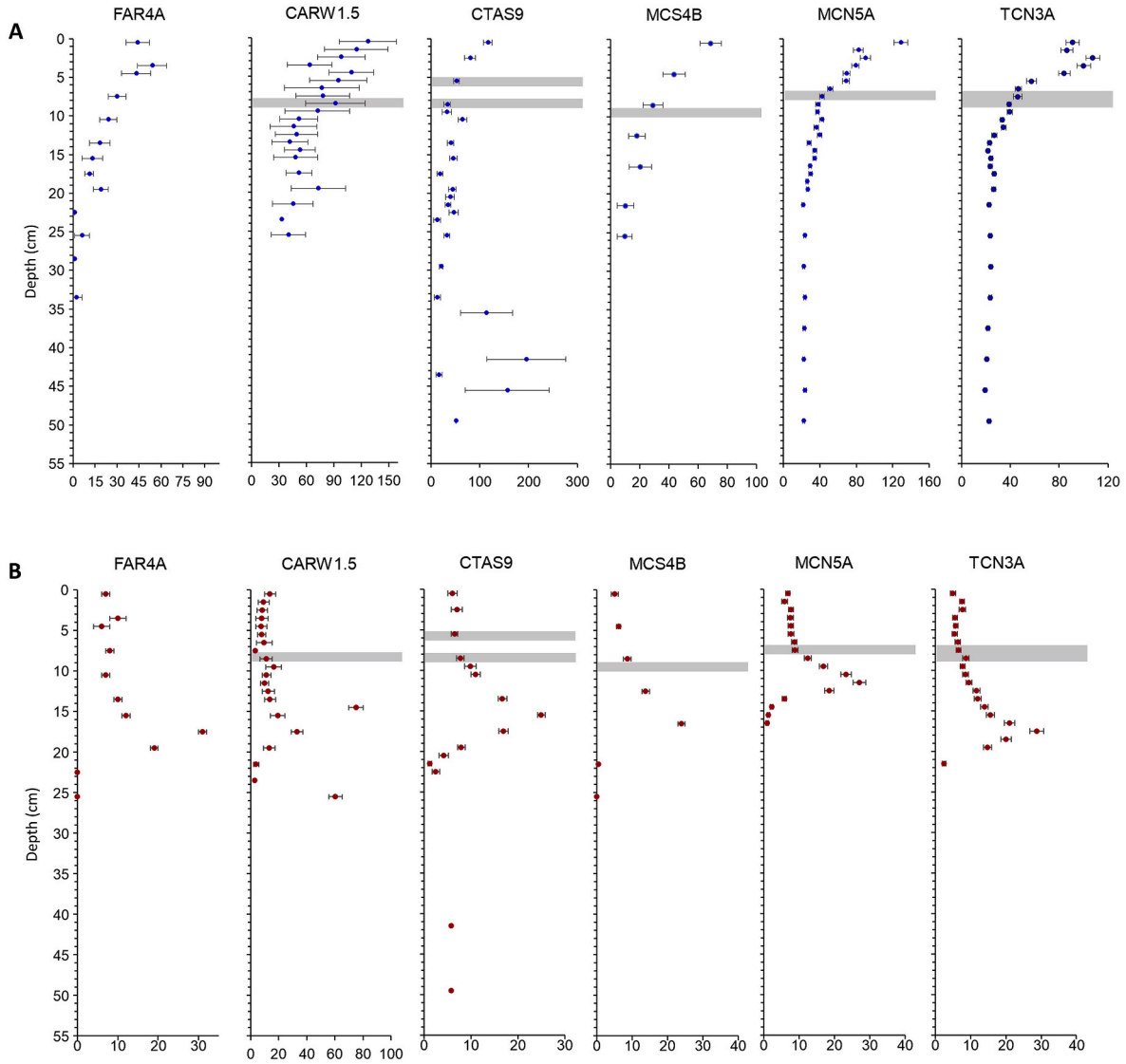

Fig. 6. Total ^{210}Pb (A) and ^{137}Cs (B) concentrations (Bq kg^{-1}) distribution with depth (cm) in the FAR4A, CARW1.5, CTAS9, MCS4B, MCN5A, and TCN3A cores from the Sado estuary. Grey bars represent the peaks of the maxima concentration of petcoke particles.

plausible origin of petcoke particles in the salt marshes studied here is fugitive emissions from activities at the port of Setúbal – loading and unloading operations, petcoke outdoor storage piles, and transport –, namely at solid bulk terminals (e.g., Eurominas and Sapec; Fig. 1B and C). Historical evidence, regarding the presence of local and regional sources, provides a chronological framework for the observed petcoke patterns in the analysed sediments. According to the data on imports, we can assign the departure from background values (i.e., prior to the increase of petcoke imports in the 1990s) to 1996 ± 2 and petcoke particle maximum concentration for the period from 2002 to 2010 (or 2006 ± 4). Therefore, we will use the maximum peak of petcoke particles in the marsh sediments as a chronological marker of a peak of anthropogenic activity corresponding to the 2006 ± 4 date. We acknowledge that the link between the source and the sink could be affected by different pathways for individual particles and depositional changes could impact the linear correlation between emissions and deposition. We discuss these potential effects below.

4.2.2. Concentration profiles of giant (63–~200 μm) spheroidal petcoke particles in the Sado core sediments

The sedimentary record of giant petcoke particles in the Sado estuary is shown in Fig. 5, presenting variations in the abundances along depth and some distinct maxima. In samples with the presence of petcoke, concentrations ranged from 1 (core FAR4A) to 4004 (core MCN5A) particles per gram of dry weight sediment (g^{-1} dry wt.; Table S4). In all but one high marsh sediment core, petcoke was not detected deep in the core, increased to a subsurface maximum, and then decreased sharply towards the core top. The three sediment cores (MCN5A, MCS4B, and TCN3A) from the Tróia spit estuarine margin, and located SW, SSW, and S of the Eurominas solid bulk terminal – where open-air petcoke stockpiling practice was maintained (Fig. 1B and C) – exhibited the highest concentrations of giant petcoke particles, 4004 particles g^{-1} dry wt. (7–8 cm depth), 3806 g^{-1} dry wt. (9–10 cm depth), and 3753 g^{-1} dry wt. (8–9 cm depth), respectively. Lower concentration peaks were observed in cores FARW1.6 (1020 g^{-1} dry wt.; 5–6 cm depth), CARW1.5 (1628 g^{-1} dry wt.; 8–9 cm depth), CTAS9 (1579 g^{-1} dry wt.; 5–6 cm depth), and FAR4A (1874 g^{-1} dry wt.; 3–4 cm depth). The FAR4A core, collected in 2005, presented an incomplete record, but the nearby core FARW1.6 (collected in 2010) suggests that FAR4A (1874 g^{-1} dry wt.; 3–4 cm depth) reflects the peak after correcting for the dates when these two cores were collected. Core CTAS9 had a secondary peak (1504 g^{-1} dry wt.; 8 cm depth) and the sample above (7 cm depth) was not analysed (Table S4), resulting in greater uncertainty when locating the peak in this core. The locations of these four cores relative to the Eurominas solid bulk terminal are N, SSE, WNW, and N, respectively. The different concentrations at each location agree with the potential transport pathways that are expected to have a greater influence on fugitive petcoke dust emissions, i.e., the prevailing wind directions – N and W quadrants. They also seem compatible with key findings from previous studies that recorded enhanced particulate levels downwind of granular material stockpiles. For instance, Sorte et al. (2018) studied the contemporary dispersion of petcoke dust (coarse particles, i.e., PM_{10}) in the port of Aveiro (Central Portugal) and Mueller et al. (2015) found fugitive similar downwind signatures from a coal stockpile due to both human activity (mechanical disturbance) and natural dust dispersion.

4.2.3. Radiometric profiles

The ^{210}Pb concentrations for the core MCN5A decreased with depth, without evidencing any major mixing or disruption in the sedimentation although there are some oscillations worth noticing from 1 to 6 cm and from 10 to 13 cm depth, with no excess ^{210}Pb below 19 cm. Core TCN3A showed evidence of mixing of the upper 5 cm, and the concentration of ^{210}Pb decreased with depth thereafter, reaching the horizon of excess ^{210}Pb at 13 cm (Fig. 6A). FAR4A ^{210}Pb profile showed departures from the expected exponential profile (potential mixing) in the upper 5 cm and at ~20 cm, but other than that it presents a generally exponential decline profile in the top ~30 cm (Freitas et al., 2008). MCS4B was sampled at a lower resolution, but we can infer a generally exponential decline profile of excess ^{210}Pb reaching beyond 25 cm. Core CARW1.5 also has a generally exponential decline profile, although irregular, that extends down to ~25 cm. Finally, CTAS9 presented subsurface activity peaks of ^{210}Pb between 35 and 46 cm. This core appears to reflect a change in the sediment fluxes, with a likely change in the source of sediments for the top 30 cm, which could be related to changes in the sedimentary dynamics on the Tróia sand spit. The upper 30 cm also shows significant variability in the ^{210}Pb activity, but the activity decreases downcore, suggesting that samples are, in general, younger towards the top of the core. The changes observed in these cores could be associated with sediment-source shifts, for instance, changes in land use (e.g., land clearance) or, in the case of CTAS9, most likely, overwash deposits. Overall, only cores CARW1.5 and MCN5A were deemed suitable for ^{210}Pb-derived chronologies based on the CRS model. Cores TCN3A and CTAS9 were deemed unreliable while FAR4A and MCS4B can only be used for linear sedimentation rates with resolutions lower than needed for this work. Following Culver et al. (2015), we modeled the theoretical ^{210}Pb down-core profile using the modern activity at each core and included in our models a simple sediment mixing layer on the top section of each core that varied in depth depending on each profile; these models are not discussed here as sediment mixing is outside the scope of the paper. Our analysis suggests that CARW1.5 models that include a sediment mixing layer better fit the $^{210}Pb_{ex}$ profile. Similar models were explored for MCN5A, but while we cannot discard sediment mixing, we were unable to fit the $^{210}Pb_{ex}$ to our alternative models that considered the effect of sediment mixing. In this paragraph, we showed the convenience of using additional tools to obtain as reliable as possible age models.

Concentration profiles of ^{137}Cs present clear subsurface peaks in all the analysed cores (Fig. 6B), at depths ranging from 11.5 cm to 17.5 cm. The differences in the depth of the peaks can be ascribed to distinct collection years, spatial variability in sedimentation rates, differential compaction, changes in the sedimentological composition, and/or changes in the sources. Given that only one peak per core was present, we assumed it corresponded to the 1963 maximum. Cs-137 was present along the cores from the maxima to the surface layers despite the significant decrease in fallout deposition, probably due to continued inputs from the catchment (e.g., Klaminder et al., 2012). Two cores, CTAS9 and CARW1.5, also present samples below the assigned 1963 horizon that are worth discussing. One single sample in CARW1.5 could be a result of downward smearing and does not seem to reflect sedimentological processes, but could also reflect bioturbation by worms, crabs, or roots where burrowed spaces are later filled with more recent materials. CTAS9 secondary maxima are associated with higher values of ^{210}Pb, these can be the result of samples from before 1963, but after 1950, although the processes reported earlier may explain their presence downcore as well. The well-preserved and clearly defined 1963-maxima and the consistent presence in all cores of this peak strongly suggest (i) a generally good potential of the high marsh sediments for discrete-event preservation, (ii) that ^{137}Cs has not been apparently disturbed in most locations (e.g., by sediment mixing), and (iii) that no significant signs of vertical mobility can be identified that would impact the identification of the 1963-maxima. Given the potential changes in sources-sinks on sediment fluxes and the potential issues with the ^{210}Pb chronological framework described above, we use here the ^{137}Cs 1963-maxima as a reference to understand the petcoke profiles. Based on ^{137}Cs 1963-maxima preservation in all the cores analysed, we consider that discrete inputs of pollutants (e.g., petcoke) that reach the high marsh settings have a potential for preservation in the sediment column and shall be valuable chronological markers, similarly to the ^{137}Cs 1963-peak. Leorri et al. (2009) had previously used artificial tracers (glass beads) to confirm that high marsh sediments have a great preservation potential despite the short-term sedimentological changes.

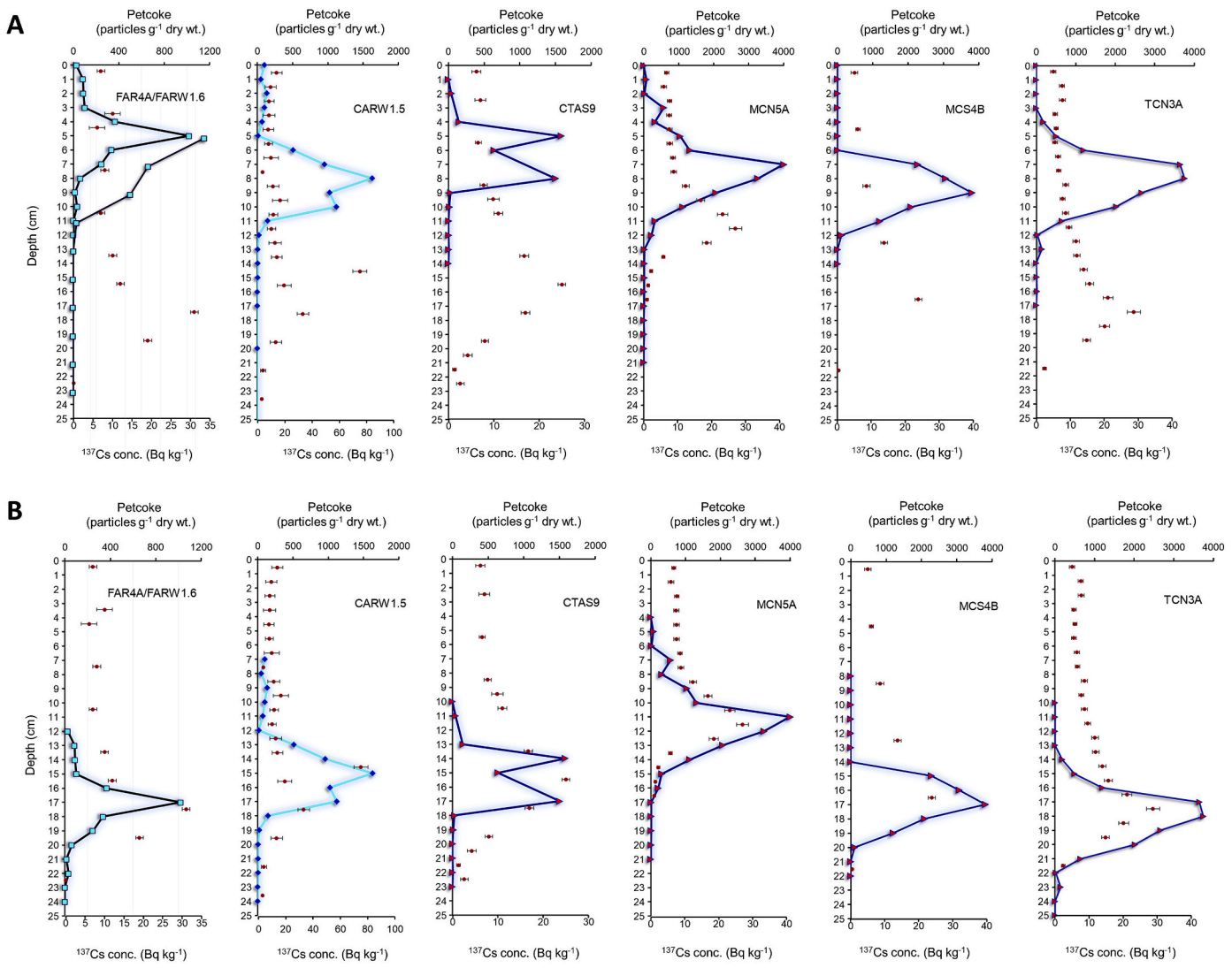

Fig. 7. A – ^{137}Cs concentrations (Bq kg^{-1}) and giant spheroidal petcoke particles (63–~200 μm) per gram of dry sediment distribution with depth (cm) in the FAR4A/FARW1.6, CARW1.5, CTAS9, MCS4B, MCN5A, and TCN3A cores from the Sado estuary. B – Same as A, but the petcoke profiles have been offset to overlap with ^{137}Cs for direct comparison.

4.2.4. Petcoke and ^{137}Cs signatures in assessing accretion rates in the Sado estuary

As shown in Fig. 5, petcoke maxima are quite distinct in the sedimentological record, concentrated in one single 1-cm thick sample in all but two cores. TCN3A recorded the peak in two contiguous samples (7.5 and 8.5 cm) and CTAS9 had two distinct peaks at 5.5 and 8.5 cm depth. Concentrations of petcoke particles remained high in the samples surrounding the maxima, with core sections recording high concentrations between 1 cm (core FARW1.6) and 5 cm (core MCN5A), as expected from the historical trends (Fig. 4). We compare ^{137}Cs and petcoke profiles to better understand the potential use of this proxy as a chronological marker. Fig. 7A presents petcoke and ^{137}Cs profiles within each core, please note that FAR4A and FARW1.6 have been combined and the depth is offset to accommodate for the different sampling years at this particular location.

On the other hand, Fig. 7B overlaps petcoke and ^{137}Cs to provide a direct correlation within each location. This direct comparison seems relevant since there is almost a decade between the setoff and the peak in both cases. Note that ^{137}Cs fallout started in the early 1950s and peaked in 1963–1964, while inputs of petcoke increased in 1994–1998 and peaked between 2002 and 2010. Both proxies have a significant decrease after their maxima due to the decline in atmospheric fallout and inputs, respectively. This exercise needs to be placed in the context of our sampling resolution (3.2 – range 2.4–11 – years per sample based on average sedimentation rates). Our comparison results in strikingly similar profiles within each core, particularly for cores CARW1.5, MCN5A, and TCN3A. These outcomes further support that the historical use of petcoke and its dispersion by winds in the region are recorded in the high marshes, where the initial appearance was recorded, followed by an increase – maxima recorded at 2006 ± 4 within 1-cm resolution –, and then a sharp reduction, providing a chronological marker for future high-resolution (sub-decadal) sedimentary research and that can support chronologies derived from the radioisotopes. Acknowledging the different sources and pathways for both markers, the goal here was to see if there were distinct maxima recorded in the sediments that can be identified as the maxima of emissions, which seems to be the case. Most cores have a depth difference between ^{137}Cs and petcoke maxima of 6–9.5 cm. However, MCN5A has a difference of only ~4 cm. In fact, there is the presence of petcoke in the same core sections where the ^{137}Cs 1963-maximum is recorded. This allowed us to identify a sedimentological disruption (unconformity), i.e., we are missing a portion of the sedimentary sequence. CARW1.5 was collected in 2010 (along with FARW1.6). The presence of the petcoke peak below 8 cm depth suggests sedimentation rates greater than 2 cm yr^{-1} for the uppermost section of

Table 2
Accretion rates and mass accumulation rates, as inferred from both ^{137}Cs and petcoke data; SWI = seawater interface (top of the core).

Core	Accretion rates (cm yr^{-1})			Mass accumulation rates (g cm^{-2} yr^{-1})	
	Petcoke−SWI	Cs137−Petcoke	Cs137−SWI	Petcoke−SWI	Cs137−SWI
FARW1.6	1.4 ± 2.8	0.3 ± 0.1[a]	0.4 ± 0.4[a]		
FAR4A	n/a	0.3 ± 0.1	0.4 ± 0.4		
CARW1.5	2.1 ± 4.1	0.1±0.0[b]	0.3 ± 0.3	0.6 ± 0.1	0.1±0.0[b]
CTAS9	0.9 ± 0.5	0.1±0.0[b]	0.3 ± 0.3		
MCN5A	0.6 ± 0.3	0.1±0.0[b]	0.2 ± 0.2	0.2±0.0[b]	0.1±0.0[b]
MCS4B	0.8 ± 0.4	0.2 ± 0.1	0.3 ± 0.3		
TCN3	0.6 ± 0.3	0.2 ± 0.1	0.3 ± 0.2	0.3±0.0[1]	0.1±0.0[b]

[a] Extrapolated from FAR4A.
[b] Less than 0.1.

this core. This enabled us to recognize a mixed layer (that we were able to model and that fits the downward ^{210}Pb profile). Similarly, FARW1.6 petcoke profiles also suggest large sedimentation rates (in the range of 1.4 cm yr^{-1}). Although unusual for long-term rates (decades to centuries), Leorri et al. (2009) reported sedimentation (burial) rates up to 6.7 cm yr^{-1} in intermediate marsh settings in a period of less than a year. This points out the value of petcoke to identify sedimentological changes at different time scales.

From the current distribution of both ^{137}Cs and petcoke we can calculate sediment accumulation rates (cm yr^{-1}) and mass accumulation rates (g cm^{-2} yr^{-1}) (Table 2). For the period covered by ^{137}Cs, linear estimates of sedimentation rates ranged from 0.2 cm yr^{-1} (MCN5A, note that this core might be missing a portion) to 0.4 cm yr^{-1} (FARW1.6–FAR4A), with most cores recording 0.3 cm yr^{-1} (CARW1.5, MCS4B, and TCN3A; CTAS9 recorded 0.3 cm yr^{-1}). Accretion rates for the period 1963–2006 (between the ^{137}Cs and petcoke maxima) varied from 0.1 to 0.3 cm yr^{-1}, with an average of 0.2 cm yr^{-1} (associated errors are 0.1 cm yr^{-1} or less). However, accretion rates were higher for the period from 2006 to the present. The average sedimentation rate was 1.1 cm yr^{-1} (range: 0.6–2.1 cm yr^{-1}). However, the errors associated with the latest period are very large and impacted by two major aspects: the short period analysed and the greater time span of petcoke emissions that limit the use of this marker at high resolution given the relatively low sedimentation rates. This discrepancy in sedimentation rates can be explained in part by changes in sediment composition. Mass accumulation rates (MARs) increased slightly from 0.1 g cm^{-2} yr^{-1} in the period from 1963 to the present to 0.2 g cm^{-2} yr^{-1} from 2006 to the present, in MCN5A. However, in TCN3A, the MAR increased from 0.1 to 0.3 g cm^{-2} yr^{-1} in the same periods, and in the core CARW1.5 from 0.1 to 0.6 g cm^{-2} yr^{-1} (almost a seven-fold increase), reflecting the thick layer of sediment deposited in a very short period, although sediment mixing needs to be considered, as indicated above. The estimate for the most recent period has a significant error (±0.1 g cm^{-2} yr^{-1}). This variability in accretion rates and MARs at different time scales is quite common in many other coastal locations as a result of human activities (dredging and sediment resuspension, changes in land use that result in greater erosion and sediment transport, physical modifications of the channels that impact the tidal wedge, etc.; e.g., Zajaczkowski et al., 2004; Du et al., 2019; Hossain et al., 2023) and emphasizes the need for additional chronological markers to strengthen chronologies in coastal systems.

5. Conclusions

The historical inputs of pollutants into coastal environments can be reconstructed using sediment records. In turn, the presence of anthropogenic signals can serve as chronological markers, providing age control to the sedimentary record, as proposed here for the green petcoke found in the high marsh sediments of the Sado estuary. In this case, petcoke particles represent a clear-cut marker of contamination by a thermal spinoff of the crude oil refining – associated with port operation atmospheric emissions – present in all seven studied sediment cores. The temporal variation of petcoke deposition reflects a rapidly increasing accumulation of petcoke closely agreeing with fast growth in both the import and use of petcoke as a fuel for co-combustion in the cement industry in the late 1990s (1996 ± 2) and peaking in 2006 ± 4. Thereafter, the sharp decline in petcoke deposition would respond to the effectiveness of implementing environmental regulations, associated with energy conversion from cement plants, the 2008 global financial crisis, and the consequent decline in petcoke imports. These sedimentary records have captured a local fingerprint of airborne pollution that fills an important gap in the reconstruction of the Sado contamination chronology, which adequately represents historical trends of industrial activity in the nearby region. Accordingly, we conclude that when identified in the sedimentological record petcoke particles can be used locally and possibly regionally to reduce chronological uncertainties and provide high-resolution accretion rates that are highly variable over different time scales. Its use needs to be supported by accurate historical data since petcoke usage and availability will be site-specific due to the diachronic aspect of its emissions. In addition, it should be considered within the context of multiple proxies, such as ^{137}Cs and total Pb, Zn concentrations, etc., to validate or support ^{210}Pb and/or ^{137}Cs derived chronologies, which can be a significant source of uncertainty in historical contamination records reconstructed from sediment cores. We caution against the use of this marker alone due to the long-time spans of these emissions, potential secondary pathways, and post-depositional changes. The results of our study also align with previous works that suggest that high marsh settings are appropriate for high-resolution environmental studies because of their good potential for preserving the sedimentological record. However, the results should be interpreted carefully (i.e., avoid overinterpretation) since our data also indicate changes in the estuarine sediment dynamics, associated with sediment-source shifts, sediment mixing/bioturbation, or a combination of both. Petcoke is a widespread contaminant that could be used globally as a chronological marker, but due to its diachronic presence, depending upon the local historical uses, its value cannot be extrapolated across regions as opposed to SCPs that have been used globally as a chronological marker in lakes (e.g., Rose, 2015). That said, SCPs should also be used with caution in areas of industrial activity since the local signal of the pollution would mask the global signal (e.g., Swindles et al., 2015), adding value to all and any chronological markers that can be identified locally, such as petcoke.

Declaration of competing interest

The authors declare that they have no known competing financial interests or personal relationships that could have appeared to influence the work reported in this paper.

Acknowledgments

The current work was carried out within the framework of the project CLIMARES – Long-term assessment of climate-induced regime shifts in Coastal Areas, PTDC/CTA-GEO/28412/2017, funded by the Portuguese Fundação para a Ciência e a Tecnologia (FCT). This work was partly funded by the Fundação para a Ciência e a Tecnologia, I.P./MCTES through national funds (PIDDAC) –UIDB/50019/2020. Funding was provided to PM through an Australian Research Council LIEF Project (LE170100219). The IAEA is grateful for the support provided to its Marine Environment Laboratories by the Government of the Principality of Monaco. Finally, the authors would like to thank the valuable comments of the anonymous reviewers, which greatly contributed to improving the manuscript.

Appendix A. Supplementary data

Supplementary data to this article can be found online at https://doi.org/10.1016/j.csr.2023.105026.

References

Al-Degs, Y.S., Ghrir, A., Khoury, H., Walker, G.M., Sunjuk, M., Al-ghouti, M.A., 2014. Characterization and utilization of fly ash of heavy fuel oil generated in power stations. Fuel Process. Technol. 123, 41–46. https://doi.org/10.1016/j.fuproc.2014.01.040.

Almeida, S.M., Silva, A.V., Freitas, M.C., Marques, A.M., Ramos, C.A., Silva, A.I., Pinheiro, T., 2012. Characterization of dust material emitted during harbour activities by k_0-INAA and PIXE. J. Radioanal. Nucl. Chem. 291, 77–82. https://doi.org/10.1007/s10967-011-1279-4.

Andrews, A., Lattanzio, R.K., 2013. Petroleum Coke: Industry and Environmental Issues. CRS, Congressional Research Service, Washington DC, USA, p. 25. CRS Report.

API, American Petroleum Institute, 2008. Petroleum Coke Category Analysis and Hazard Characterization. Petroleum HPV Testing Group, Consortium Registration # 1100997, p. 36.

Appleby, P.G., 2008. Three decades of dating recent sediments by fallout radionuclides: a review. Holocene 18, 83–93. https://doi.org/10.1177/0959683607085598.

Bacci, P., Del Monte, M., Longhetto, A., Piano, A., Prodi, F., Redaelli, P., Sabbioni, C., Ventura, A., 1983. Characterization of the particulate emission by a large oil fired power plant. J. Aerosol Sci. 14, 557–572. https://doi.org/10.1016/0021-8502(83)90011-3.

Barst, B.D., Ahad, J.M.E., Rose, N.L., Jautzy, J.J., Drevnick, P.E., Gammon, P.R., Sanei, H., Savard, M.M., 2017. Lake-sediment record of PAH, mercury, and fly-ash particle deposition near coal-fired power plants in Central Alberta, Canada. Environ. Pollut. 231, 644–653. https://doi.org/10.1016/j.envpol.2017.08.033.

Barwise, A.J.G., 1990. Role of nickel and vanadium in petroleum classification. Energy Fuels 4, 647–652. https://doi.org/10.1021/ef00024a005.

Basha, S.I., Aziz, A., Maslehuddin, M., Ahmad, S., Hakeem, A.S., Rahman, M.M., 2020. Characterization, processing, and application of heavy fuel oil ash, and industrial waste material – a review. Chem. Rec. 20, 1568–1595. https://doi.org/10.1002/tcr.202000100.

Bindler, R., Renberg, I., Appleby, P.G., Anderson, N.J., Rose, N.L., 2001. Mercury accumulation rates and spatial patterns in lake sediments from west Greenland: a coast to ice margin transect. Environ. Sci. Technol. 35, 1736–1741. https://doi.org/10.1021/es0002868.

Buffoni, G., Schirone, A., Delfanti, R., 2020. A numerical investigation for dating ^{210}Pbex and ^{137}Cs vertical profiles in a coastal area: the Eastern Ligurian Sea, Italy. J. Environ. Radioact. 212, 106122 https://doi.org/10.1016/j.jenvrad.2019.106122.

Cabrita, M.T., Brito, P., Caçador, I., Duarte, B., 2020. Impacts of phytoplankton blooms on trace metal recycling and bioavailability during dredging events in the Sado estuary (Portugal). Mar. Environ. Res. 153, 104837 https://doi.org/10.1016/j.marenvres.2019.104837.

Caeiro, S., Costa, M.H., Ramos, T.B., Fernandes, F., Silveira, N., Coimbra, A., Medeiros, G., Painho, M., 2005. Assessing heavy metal contamination in Sado estuary sediment: an index analysis approach. Ecol. Indicat. 5, 151–169. https://doi.org/10.1016/j.ecolind.2005.02.001.

Caeiro, S., Costa, M.H., DelValls, A., Repolho, T., Gonçalves, M., Mosca, A., Coimbra, A. P., Ramos, T.B., Painho, M., 2009. Ecological risk assessment of sediment management areas: application to Sado Estuary, Portugal. Ecotoxicology 18, 1165–1175. https://doi.org/10.1007/s10646-009-0372-8.

Caruso, J.A., Zhang, K., Schroeck, N.J., McCoy, B., McElmurry, S.P., 2015. Petroleum coke in the urban environment: a review of potential health effects. Int. J. Environ. Res. Publ. Health 12, 6218–6231. https://doi.org/10.3390/ijerph120606218.

Cearreta, A., Irabien, M.J., Leorri, E., Yusta, I., Croudace, I.W., Cundy, A.B., 2000. Recent anthropogenic impacts on the Bilbao estuary, Northern Spain: geochemical and microfaunal evidence. Estuar. Coast Shelf Sci. 50, 571–592. https://doi.org/10.1006/ecss.1999.0582.

Cearreta, A., Irabien, M.J., Leorri, E., Yusta, I., Quintanilla, A., Zabaleta, A., 2002. Environmental transformation of the Bilbao estuary, N. Spain: microfaunal and geochemical proxies in the recent sedimentary record. Mar. Pollut. Bull. 44, 487–503. https://doi.org/10.1016/S0025-326X(01)00261-2.

CONCAWE, 1993. Petroleum Coke. CONCAWE, Brussels, Belgium. Report no. 93/105.

Costa, P.M., Neuparth, T.S., Caeiro, S., Lobo, J., Martins, M., Ferreira, A.M., Caetano, M., Vale, C., DelValls, A., Costa, M.H., 2011. Assessment of the genotoxic potential of contaminated estuarine sediments in fish peripheral blood: laboratory versus *in situ* studies. Environ. Res. 111, 25–36. https://doi.org/10.1016/j.envres.2010.09.011.

Costa, M., Arruda, A.M., Dias, L., Barbosa, R., Mirão, J., Vandenabeele, P., 2019. The combined use of Raman and micro-X-ray diffraction analysis in the study of archaeological glass beads. J. Raman Spectrosc. 50, 250–261. https://doi.org/10.1002/jrs.5446.

Culver, S.J., Leorri, E., Mallinson, D.J., Corbett, D.R., Shazili, N.A.M., 2015. Recent coastal evolution and sea-level rise, Setiu Wetland, Peninsular Malaysia. Palaeogeogr. Palaeoclimatol. Palaeoecol. 417, 406–421. https://doi.org/10.1016/j.palaeo.2014.10.001.

Dias, E.B., Alves, J.F., 2010. Ports, policies, and interventions in ports in Portugal – 20th century. URL Cah. Méditerranée 80, 36–60. https://doi.org/10.4000/cdlm.5131. journals.openedition.org/cdlm/5131, ISSN: 1773-0201.

Doubleday, N.C., Douglas, M.S.V., Smol, J.P., 1995. Paleoenvironmental studies of black carbon deposition in the High Arctic: a case study from Northern Ellesmere Island. Sci. Total Environ. 160–161, 661–668. https://doi.org/10.1016/0048-9697(95)04400-U.

Dourson, M.L., Chinkin, L.R., MacIntosh, D.L., Finn, J.A., Brown, K.W., Reid, S.B., Martinez, J.M., 2016. A case study of potential human health impacts from petroleum coke transfer facilities. J. Air Waste Manag. Assoc. 66, 1061–1076. https://doi.org/10.1080/10962247.2016.1180328.

Du, J., Guan, D., Yao, Z., Wang, Z., Huo, C., 2019. Records of human-induced changes in sedimentation and carbon sequestration in Dalian Bay, north China. Continent. Shelf Res. 178, 51–58. https://doi.org/10.1016/j.csr.2019.04.004.

Edwards, L., 2015. The history and future challenges of calcined petroleum coke production and use in aluminum smelting. JOM 67, 308–321. https://doi.org/10.1007/s11837-014-1248-9.

EPA, 1978. United States Environmental Protection Agency, EPA-600/7-78-071. Particulate Control for Fugitive Dust, p. 57.

Freitas, M.C., Andrade, C., Cruces, A., Munhá, J., Sousa, M.J., Moreira, S., Jouanneau, J. M., Martins, L., 2008. Anthropogenic influence in the Sado estuary (Portugal): a geochemical approach. J. Iber. Geol. 34, 271–286. https://doi.org/10.5209/JIGE.33892.

Furieri, B., Santos, J.M., Russeil, S., Harion, J.-L., 2014. Aeolian erosion of storage piles yards: contribution of the surrounding areas. Environ. Fluid Mech. 14, 51–67. https://doi.org/10.1007/s10652-013-9293-4.

García-Artola, A., Cearreta, A., Leorri, E., 2015. Relative sea-level changes in the Basque coast (northern Spain, Bay of Biscay) during the Holocene and Anthropocene: the Urdaibai estuary case. Quat. Int. 364, 172–180. https://doi.org/10.1016/j.quaint.2014.06.040.

García-Artola, A., Cearreta, A., Irabien, M.J., Leorri, E., Sanchez-Cabeza, J.-A., Corbett, D.R., 2016. Agricultural fingerprints in salt-marsh sediments and adaptation to sea-level rise in the eastern Cantabrian coast (N. Spain). Estuar. Coast Shelf Sci. 171, 66–76. https://doi.org/10.1016/j.ecss.2016.01.031.

Gonçalves, C., Brogueira, M.J., Nogueira, M., 2015. Tidal and spatial variability of nitrous oxide (N_2O) in Sado estuary (Portugal). Estuar. Coast Shelf Sci. 167, 466–474. https://doi.org/10.1016/j.ecss.2015.10.028.

Hicks, S., Isaksson, E., 2006. Assessing source areas of pollutants from studies of fly ash, charcoal, and pollen from Svalbard snow and ice. J. Geophys. Res. 111, D02113 https://doi.org/10.1029/2005JD006167.

Holsen, T.M., Noll, K.E., 1992. Dry deposition of atmospheric particles: application of current models to ambient data. Environ. Sci. Technol. 25, 1807–1815. https://doi.org/10.1021/es00033a015.

Hossain, M.S., Yasir, M., Shahriar, M.S., Jahan, M., Liu, S., Niang, A.J., 2023. Morphological change assessment of a coastal island in SE Bangladesh reveals high accumulation rates. Regional Studies in Marine Science, 102969. https://doi.org/10.1016/j.rsma.2023.102969.

Inácio, M., Freitas, M.C., Cunha, A.G., Antunes, C., Leira, M., Lopes, V., Andrade, C., Silva, T.A., 2022. Simplified Marsh Response Model (SMRM): a methodological approach to quantify the evolution of salt marshes in a sea-level rise context. Remote Sens 14, 3400. https://doi.org/10.3390/rs14143400.

INE, Instituto Nacional de Estatística, 2019. Anuário Estatístico da Área Metropolitana de Lisboa, 2018. Lisboa: INE, 2019. Disponível na. https://www.ine.pt/xurl/pub/410495118. ISSN 2183-6876. ISBN 978-989-25-0505-3.

Inoue, J., Takenaka, N., Okudaira, T., Kuwae, M., 2022. The Record of Sedimentary Spheroidal Carbonaceous Particles (SCPs) in Beppu Bay, Southern Japan, Compared to Historical Trends of Industrial Activity and Atmospheric Pollution: Further Evidence for SCPs as a Marker for Anthropocene Industrialization. The Anthropocene Review. https://doi.org/10.1177/20530196221076577.

Irabien, M.J., García-Artola, A., Cearreta, A., Leorri, E., 2015. Chemostratigraphic and lithostratigraphic signatures of the Anthropocene in estuarine areas from the eastern Cantabrian coast (N. Spain). Quat. Int. 364, 196–205. https://doi.org/10.1016/j.quaint.2014.08.056.

Jaenicke, R., 1980. Atmospheric aerosols and global climate. J. Aerosol Sci. 11, 577–588. https://doi.org/10.1007/978-94-009-8514-8_33.

Jariyasopit, N., Zhang, Y., Martin, J.W., Harner, T., 2018. Comparison of polycyclic aromatic compounds in air measured by conventional passive air samplers and passive dry deposition samplers and contributions from petcoke and oil sands ore. Atmos. Chem. Phys. 18, 9161–9171. https://doi.org/10.5194/acp-18-9161-2018.

Kameshkov, A.V., Rudko, V.A., Gabdulkhakov, R.R., Nazarenko, M.Y., Starkov, M.K., Povarov, V.G., Pyagay, I.N., 2021. Technology of producing petroleum coking

additives to replace coking coal. ACS Omega 6, 35307–35314. https://doi.org/10.1021/acsomega.1c04075.
Kemp, A.C., Kegel, J.J., Culver, S.J., Barber, D.C., Mallinson, D.J., Leorri, E., Bernhardt, C.E., Cahill, N., Riggs, S.R., Woodson, A.L., Mulligan, R.P., Horton, B.P., 2017. Extended late Holocene relative sea-level histories for North Carolina, USA. Quat. Sci. Rev. 160, 13–30. https://doi.org/10.1016/j.quascirev.2017.01.012.
Kiciński, W., Dyjak, S., 2020. Transition metal impurities in carbon-based materials: pitfalls, artifacts, and deleterious effects. Carbon 168, 748–845. https://doi.org/10.1016/j.carbon.2020.06.004.
Klaminder, J., Appleby, P., Crook, P., Renberg, I., 2012. Post-deposition diffusion of ^{137}Cs in lake sediment: implications for radiocaesium dating. Sedimentology 59, 2259–2267. https://doi.org/10.1111/j.1365-3091.2012.01343.x.
Kuo, J., 2018. Air Pollution Control: Engineering for Environmental Engineers. CRC Press, Taylor & Francis Group, p. 368. https://doi.org/10.1201/9780429185793.
Lee, J.M., Baker, J.J., Murray, D., Llerena, R., Rolle, J.G., 1997. Quality analysis of petroleum cokes and coals for export specifications required in use of specialty products and utility fuels. 214th National Meeting, American Chemical Society 42, 844–853.
Leorri, E., Martin, R.E., Horton, B.P., 2009. Field experiments on bioturbation in salt marshes (Bombay Hook National Wildlife Refuge, Smyrna, DE, USA): implications for sea-level studies. J. Quat. Sci. 24, 139–149. https://doi.org/10.1002/jqs.1183.
Leorri, E., Cearreta, A., Corbett, D.R., Blake, W.H., Fatela, F., Gehrels, R., Irabien, M.J., 2010. Identification of suitable areas for high-resolution sea-level studies in SW Europe using commonly applied ^{210}Pb models. Geogaceta 48, 35–38. ISSN: 0213-683X.
Leorri, E., Cearreta, A., García-Artola, A., Irabien, M.J., Blake, W.H., 2013. Relative sea-level rise in the Basque coast (N Spain): different environmental consequences on the coastal area. Ocean Coast Manag. 77, 3–23. https://doi.org/10.1016/j.ocecoaman.2012.02.007.
Leorri, E., Cearreta, A., Irabien, M.J., García-Artola, A., Corbett, D.R., Horsman, E., Blake, W.H., Sanchez-Cabeza, J.A., 2014a. Anthropogenic disruptions of the sedimentary record in coastal marshes: Examples from the southern Bay of Biscay (N. Spain). Continent. Shelf Res. 86, 132–140. https://doi.org/10.1016/j.csr.2013.08.016.
Leorri, E., Mitra, S., Irabien, M.J., Zimmerman, A.R., Blake, W.H., Cearreta, A., 2014b. A 700-year record of combustion-derived pollution in northern Spain: tools to identify the Holocene/Anthropocene transition in coastal environments. Sci. Total Environ. 470–471, 240–247. https://doi.org/10.1016/j.scitotenv.2013.09.064.
Lewan, M.D., 1984. Factors controlling the proportionality of vanadium and nickel in crude oils. Geochem. Cosmochim. Acta 48, 2231–2238. https://doi.org/10.1016/0016-7037(84)90219-9.
Lillebø, A.I., Coelho, P.J., Pato, P., Válega, M., Margalho, R., Reis, M., Raposo, J., Pereira, E., Duarte, A.C., Pardal, M.A., 2011. Assessment of mercury in water, sediments, and biota of a Southern European Estuary (Sado Estuary, Portugal). Water Air Soil Pollut. 214, 667–680. https://doi.org/10.1007/s11270-010-0457-2.
Lin, C.Y.-Y., Edvinsson, L., Chen, J., Beding, T., 2013. Impact of the 2008 global financial crisis. In: National Intellectual Capital and the Financial Crisis in Greece, Italy, Portugal, and Spain, vol. 7. Springer Briefs in Economics, New York, pp. 5–15. https://doi.org/10.1007/978-1-4614-5990-3_2. Springer.
López, L., Lo Mónaco, S., 2017. Vanadium, nickel and sulfur in crude oils and source rocks and their relationship with biomarkers: implications for the origin of crude oils in Venezuelan basins. Org. Geochem. 104, 53–68. https://doi.org/10.1016/j.orggeochem.2016.11.007.
Lu, X., Matsumoto, E., 2005. Recent sedimentation rates derived from ^{210}Pb and ^{137}Cs methods in Ise Bay, Japan. Estuar. Coast Shelf Sci. 65, 83–93. https://doi.org/10.1016/j.ecss.2005.05.009.
Mancuso, L., Arienti, S., 2017. Petroleum coke (Petcoke) and refinery residues. In: Wang, T., Stiegel, G. (Eds.), Integrated Gasification Combined (IGCC) Technologies. Woodhead Publishing, Cambridge, pp. 121–144.
Martins, C.C., Bícego, M.C., Rose, N.L., Taniguchi, S., Lourenço, R.A., Figueira, Rubens C. L., Mahiques, M.M., Montone, R.C., 2010. Historical record of polycyclic aromatic hydrocarbons (PAHs) and spheroidal carbonaceous particles (SCPs) in marine sediment cores from Admiralty Bay, King George Island, Antarctica. Environ. Pollut. 158, 192–200. https://doi.org/10.1016/j.envpol.2009.07.025.
Maxim, L.D., Galvin, J.B., Niebo, R., Segrave, A.M., Kampa, O.A., Utell, M.J., 2006. Occupational exposure to carbon/coke fibers in plants that produce green or calcined petroleum coke and potential health effects: 2. Fiber Concentrations. Inhal. Toxicol. 18, 17–32. https://doi.org/10.1080/08958370500282258.
McCrone, W.G., Delly, J.G., 1973. The Particle Atlas, II. Ann Arbor Science, Ann Arbor, p. 267.
McKee, R.H., Herron, D., Beatty, P., Podhasky, P., Hoffman, G.M., Swigert, J., Lee, C., Wong, D., 2014. Toxicological assessment of green petroleum coke. Int. J. Toxicol. 33, 156S–167S. https://doi.org/10.1177/1091581813504187.
Milan, C.S., Swenson, E.M., Turner, R.E., Lee, J.M., 1995. Assessment of the ^{137}Cs method for estimating sediment accumulation rates: Louisiana salt marshes. J. Coast Res. 11, 296–307. http://www.jstor.org/stable/4298341.
MOECC, 2017. Management Approaches for Industrial Fugitive Dust Sources. MOECC Technical Bulletin, Ontario, Canada, p. 18.
Moreira, S., Freitas, M.C., Araújo, M.F., Andrade, C., Munhá, J., Fatela, F., Cruces, A., 2009. Contamination of intertidal sediments -the case of Sado estuary (Portugal). J. Coast Res. 56, 1380–1384. http://www.jstor.org/stable/25738015.
Moreno, J., Fatela, F., Leorri, E., Moreno, F., Freitas, M.C., Valente, T., Araújo, M.F., Gomez-Navarro, J.J., Guise, L., Blake, W.H., 2017. Bromine soil/sediment enrichment in tidal salt marshes as a potential indicator of climate changes driven by solar activity: new insights from W coast Portuguese estuaries. Sci. Total Environ. 580, 324–338. https://doi.org/10.1016/j.scitotenv.2016.11.130.
Mueller, S.F., Mallard, J.W., Mao, Q., Shaw, S.L., 2015. Emission factors for fugitive dust from bulldozers working on a coal pile. J. Air Waste Manag. Assoc. 65, 27–40. https://doi.org/10.1080/10962247.2014.960953.
Novak, L., Bizjan, B., Pražnikar, J., Horvat, B., Orbanić, A., Širok, B., 2015. Numerical modeling of dust lifting from a complex-geometry industrial stockpile. J. Mech. Eng. 61, 621–631. https://doi.org/10.5545/sv-jme.2015.2824.
Olszewski, G., Andersson, P., Lindahl, P., Eriksson, M., 2018. On the distribution and inventories of radionuclides in dated sediments around the Swedish coast. J. Environ. Radioact. 186, 142–151. https://doi.org/10.1016/j.jenvrad.2017.09.025.
Pereira, F.M., Caeiro, S., Costa, M., Costa, P.M., 2014. Development of an integrative approach for the characterization of environmental risk on marine transition ecosystems: the Sado estuary as a case study. Front. Mar. Sci. Conference Abstract: IMMR | International Meeting on Marine Research. https://doi.org/10.3389/conf.fmars.2014.02.00038, 2014.
Pereira, T.C., Pina, A., Canaveira, P., Amaro, A., Borges, M., Silva, R., 2020. Portuguese Informative Inventory Report 1990–2018. Submitted under the NEC Directive (EU) 2016/2284 and the UNECE Convention on Long-Range Transboundary Air Pollution. Portuguese Environmental Agency, Amadora, Portugal.
Petroleum Coke Group, 2020. Draft Screening Assessment, Chemical Abstracts Service Registry Numbers 64741-79-3 and 64743-05-1. Government of Canada, p. 43. https://www.canada.ca/content/dam/eccc/documents/pdf/pded/petroleum-coke/Draft-screening-assessment-petroleum-coke-group.pdf.
Picón-Hernández, H.J., Centeno-Hurtado, A., Pantoja-Agreda, E.F., 2008. Morphological classification of coke formed from the Castilla and Jazmin crude oils. C.T. F Ciencia, Tecnol., Futuro 3, 7–20.
PROMAN, 2016. Melhoria da Acessibilidade Marítima ao Porto de Setúbal. T. 15006 MEMÓRIA DESCRITIVA E JUSTIFICATIVA 1, pp. 1–39.
Quintas, M.C., 2011. Porto de Setúbal. Um actor de desenvolvimento. Editora APSS, SA Administração dos Portos de Setúbal e Sesimbra, SA, Setúbal, p. 354.
Rose, N.L., 2015. Spheroidal carbonaceous fly ash particles provide a globally synchronous stratigraphic marker for the Anthropocene. Environ. Sci. Technol. 49, 4155–4162. https://doi.org/10.1021/acs.est.5b00543.
Rose, N.L., Appleby, P.G., 2005. Regional applications of lake sediment dating by spheroidal carbonaceous particle analysis I: United Kingdom. J. Paleolimnol. 34, 349–361.
Rose, N.L., Harlock, S., Appleby, P.G., 1999. The spatial and temporal distributions of spheroidal carbonaceous fly-ash particles (SCP) in the sediment records of European mountain lakes. Water Air Soil Pollut. 113, 1–32. https://doi.org/10.1023/A:1005073623973.
Rose, N.L., Flower, R.J., Appleby, P.G., 2003. Spheroidal carbonaceous particles (SCPs) as indicators of atmospherically deposited pollutants in North African wetlands of conservation importance. Atmos. Environ. 37, 1655–1663. https://doi.org/10.1016/S1352-2310(03)00012-8.
Rose, N.L., Jones, V.J., Noon, P.E., Hodgson, D.A., Flower, R.J., Appleby, P.G., 2012. Long-range transport of pollutants to the Falkland Islands and Antarctica: Evidence from lake sediment fly ash particle records. Environ. Sci. Technol. 46, 9881–9889. https://doi.org/10.1021/es3023013.
Rosenberg, P.D., Parker, D.J., Ryder, C., Marsham, J.H., Garcia-Carreras, L., Dorsey, J.R., Brooks, I.M., Dean, A.R., Crosier, J., McQuaid, J.B., Washington, R., 2014. Quantifying particle size and turbulent scale dependence of dust uplift in the Sahara using aircraft measurements. J. Geophys. Res. Atmos. 119, 7577–7598. https://doi.org/10.1002/2013JD021255.
Ruppel, M., Lund, M.T., Grythe, H., Rose, N.L., Weckström, J., Korhola, A., 2013. Comparison of Spheroidal Carbonaceous Particle Data with Modelled Atmospheric Black Carbon Concentration and Deposition and Air Mass Sources in Northern Europe, 1850–2010. *Advances in Meteorology* 2013. https://doi.org/10.1155/2013/393926. Article ID 393926.
Sanchez-Cabeza, J.A., Masqué, P., Ani-Ragolta, I., 1998. ^{210}Pb and ^{210}Po analysis in sediments and soils by microwave acid digestion. J. Radioanal. Nucl. Chem. 227, 19–22. https://doi.org/10.1007/BF02386425.
Santos, A.R., Silva, R.J., Renó, M.L.G., 2015. Analysis of petroleum coke consumption in some industrial sectors. Journal of Petroleum Science Research 1, 1–7. https://doi.org/10.12783/jpsr.2015.0401.01.
Serafim, A., Company, R., Lopes, B., Pereira, C., Cravo, A., Fonseca, V.F., França, S., Bebianno, M.J., Cabral, H.N., 2013. Evaluation of sediment toxicity in different Portuguese estuaries: ecological impact of metals and polycyclic aromatic hydrocarbons. Estuar. Coast Shelf Sci. 130, 30–41. https://doi.org/10.1016/j.ecss.2013.04.018.
Shawabkeh, R., Khan, M.J., Al-Juhani, A.A., Wahhab, H.I.Al-A., Hussein, I.A., 2011. Enhancement of surface properties of oil fly ash by chemical treatment. Appl. Surf. Sci. 258, 1643–1650. https://doi.org/10.1016/j.apsusc.2011.07.136.
Sorte, S., Lopes, M., Rodrigues, V., Leitão, J., Monteiro, A., Ginja, J., Coutinho, M., Borrego, C., 2018. Measures to reduce air pollution caused by fugitive dust emissions from harbour activities. International Journal of Environmental Impacts 1, 115–126. https://doi.org/10.2495/EI-V1-N2-115-126.
Stockman, L., 2013. Petroleum coke: the coal Hiding in the tar Sands. Available online: http://priceofoil.org/2013/01/17/petroleumcoke-the-coal-hiding-in-the-tar-sands/. (Accessed 17 June 2021).
Swindles, G.T., Watson, E., Turner, T.W., Galloway, J.M., Hadlari, T., Wheeler, J., Bacon, K.L., 2015. Spheroidal carbonaceous particles are a defining stratigraphic marker for the Anthropocene. Sci. Rep. 5, 10264 https://doi.org/10.1038/srep10264.
Tillman, D.A., Duong, D.N.B., Harding, N.S., 2012. Waste fuel–coal blending. In: Tillman, D.A., Duong, D.N.B., Harding, N.S. (Eds.), Solid Fuel Blending. Butterworth-Heinemann, pp. 31–70. https://doi.org/10.1016/B978-0-12-380932-2.00002-7.

Van der Does, M., Knippertz, P., Zschenderlein, P., Giles Harrison, R., Stuut, J.-B.W., 2018. The mysterious long-range transport of giant mineral dust particles. Sci. Adv. 4, eaau2768 https://doi.org/10.1126/sciadv.aau2768.

Zajaczkowski, M., Szczucinski, W., Bojanowski, R., 2004. Recent changes in sediment accumulation rates in Adventfjorden, Svalbard. Oceanologia 46, 217–231.

Zhang, Y., Shotyk, W., Zaccone, C., Noernberg, T., Pelletier, R., Bicalho, B., Froese, D.G., Davies, L., Martin, J.W., 2016. Airborne petcoke dust is a major source of polycyclic aromatic hydrocarbons in the Athabasca Oil Sands region. Environ. Sci. Technol. 50, 1711–1720. https://doi.org/10.1021/acs.est.5b05092.